



Contents lists available at [Egyptian Knowledge Bank](https://www.egyptianknowledgebank.com)

# Advances in Environmental and Life Sciences

journal homepage: <https://aels.journals.ekb.eg>



## Magnetite/Reduced Graphene Oxide Synthesis and Study as a Potential Adsorbent for Absorptive Removal of Heavy Metals

Sherif F T Eldamhogy<sup>a,\*</sup>, Sabry A Elkorashy<sup>a</sup>, Hesham R Tantawy<sup>b</sup>, Nadia F Abdel Aal<sup>a</sup>

<sup>a</sup>Chemistry Department, Faculty of Science, Suez Canal University, 41522, Ismailia, Egypt

<sup>b</sup>Chemical engineering department, Military Technical college

### Abstract

Owing to its exceptional properties, graphene, a planar layer of  $sp^2$ -bonded carbon atoms, attracted interest of researchers. A distinct matrix for nanocomposites, graphene has exceptional chemical endurance, high surface/volume ratio, and strong electrical conductivity. Due of their versatility, research in recent years has focused on incorporating graphene with appropriate materials. In this study, Improved Hummer method utilized in synthesizing graphene oxide (GO). An appropriate chemical reducing agent was used to synthesize (RGO). Magnetite was prepared from ferrous ammonium sulfate and  $((NH_4)_2Fe(SO_4)_2 \cdot 6H_2O)$  to ferric chloride ( $FeCl_3 \cdot 6H_2O$ ), then by co-precipitation method. Magnetite Reduced Graphene Oxide (MRG) was synthesized with different amounts of RGO relative to magnetite (5, 10, and 30% wt. %) to prepare (MRG 5, 10, and 30%). Samples were morphologically characterized using a (HRTEM). Additionally, Raman and FTIR spectroscopy were used to identify the samples' chemical composition. Using (XRD), samples' crystallographic was identified. To ascertain the magnetic behavior, (VSM) was employed. Furthermore, fluctuation in metal ions concentration vs adsorption time was studied by UV-VIS spectrophotometer. Research findings demonstrated produced nano-composites' great adsorption potential even higher than both RGO and magnetite, the nano-composites demonstrated a synergistic effect that enhanced the composite's adsorption effectiveness. A 30% RGO sample was found to have the max adsorption activity for Cr (VI), Cu (II), and Mn (VII) with values of % removal 68, 80, and 70% respectively at PH =9 which make (MRG30) the ideal sample for heavy metal removal.

**Keywords:** Graphene, Magnetite Reduced Graphene oxide composite, Adsorption, Wastewater treatment, Removal of Heavy metals

### 1. Introduction:

Environment is constantly degraded as a result of the world's expanding population and rising human activity such as urbanism & industry [1]. Heavy metal pollution, usually from industrial effluents, is a serious ecological hazard. Cd, Cu, Hg, Pb, Cr, As, and other heavy metals are discharged into the aquatic environment. The chemical stability and lack of biodegradability of heavy metals,

allowing them to persistent accumulation in environment. Exposure to hazardous heavy metals for a long time or at a high level can cause a variety of serious health issues, including brain impairment, anemia, bone defects, and cancer [2]. As a result, efficient approaches for extracting heavy metal pollution are desperately needed.

Among various Heavy metal removal methods used, the adsorption approach is favored among these techniques owing of its merits, as well as its cheap cost, great efficiency, and simplicity of use. For wastewater treatment, different adsorbents were used, including activated carbon [3],

\* Corresponding author.

Email address: [sherifeldamhogy@gmail.com](mailto:sherifeldamhogy@gmail.com) (Sherif F Eldamhogy)

chitosan [4], biochar [5], zeolite [6], polymer [7], carbon nanotube [8], metal-organic frameworks (MOFs) [9], carbon quantum dots (CQDs) [10], and graphene [11]. Recently, there's been a significant interest in graphene-based nanomaterials as highly efficient adsorbents for extracting heavy metals from water. [12–22].

Graphene oxide (GO) serves as the manufacturing basis for several graphene-based products. GO prepared via Improved Hummer method using strong oxidative conditions to exfoliate raw graphite [23]. During the production of GO, several oxygen-ous groups are added to the aromatic ring, including carbonyl, carboxyl, hydroxyl, and epoxy, making GO extremely hydrophilic and forming stably distributed hydrosol. Because of the abundance of oxygen-ous groups and conjugated electrons, GO- Based materials can engage in interactions via hydrogen bonds, and electrostatic attraction with inorganic or organic contaminants. [12, 13]. However, GO's evenly dispersed structure has both benefits and drawbacks. Proper distribution enhances the adsorption potential by sufficiently exposing the adsorption sites of GO to contaminants. But, well dispersion makes the recovery of GO is extremely difficult, resulting in lower recycling efficiency and additional contamination.

Magnetic particles were employed to counteract this disadvantage in order to facilitate recovery of adsorbent. Because of its ease of manufacturing, superior biocompatibility, and inexpensive cost,  $\text{Fe}_3\text{O}_4$  [13–15, 24–27, 46], has attracted the curiosity of researchers. Synthesis of magnetite/RGO nano-composite, which have fascinating conduction properties, enormous surface area, a flatter form, cheap cost, a powerful magnetic field and environmental safety. [28–31]. Magnetite nano particles and graphene merged together forming RGO/  $\text{Fe}_3\text{O}_4$  nano-composite exhibiting recognizable features like great extractability, magnetization, significant surface area, and considerable dispersibility [32]. Through degradation, RGO/ $\text{Fe}_3\text{O}_4$  nano-composite may effectively eliminate harmful heavy metals [30, 33].

$\text{Fe}_3\text{O}_4$  serves four tasks in the GO/ $\text{Fe}_3\text{O}_4$  system: (1) Simplifies separation and recovery. (2) The strong  $\pi$ - $\pi$  interaction provides steric hin-

drance to graphene sheet restacking and aggregation. (3) It has adsorption capacity. (4) Attachment to graphene sheets prevents  $\text{Fe}_3\text{O}_4$  aggregation.

Generally, aqueous solution and adsorbent material are segregated using centrifugation and filtration treatments. [34]. In comparison with other removal techniques, after finishing the adsorption stage, magnetic separation is a reliable, fast, and economic procedure for removing magnetic adsorbents from the medium. [35]. As a result, it is beneficial to develop rGO/  $\text{Fe}_3\text{O}_4$  NCs which is characterized by magnetic separation and have high surface area for the removal of water contaminants.

The following are the three goals of this work: (1) synthesis a highly effective adsorbent for heavy metals from the aqueous solutions based on the rGO/  $\text{Fe}_3\text{O}_4$  configuration with high ability of adsorption and ease of separation. (2) Characterization of the fabricated composites to reveal its morphological, chemical & physical properties which is responsible for its adsorption efficiency and (3) Studying the adsorption efficiency of RGO/ Magnetite RGO composite toward the Cr(VI), Cu (II) and Mn(VII) in aqueous solution. Cr (VI), Cu (II) and Mn (VII) was selected as models. The findings of this study may encourage the use of the rGO/  $\text{Fe}_3\text{O}_4$  design as a possible adsorbent.

## 2. Experimental methodology:

### 2.1. Materials:

Chemicals used were reagent-grade. They were required with some specified purities from the given sources and utilized without further purifications.

### 2.2. Graphene oxide / reduced graphene oxide Synthesize:

GO synthesized by via Hummers technique [36]. RGO was prepared from GO utilizing Ascorbic acid as a reductant. For 15 minutes, GO samples were dispersed in 100mL distilled water before being repeated four times. Solution sample was then transferred to a 2L baker and mechanically stirred for 24 hours with 1L distilled water. The reducing agent was gradually added to the suspension after

it had been heated to 70 °C for about 1 hour. After that, the solution was mechanically stirred for 24 hours [37].

### 2.3. RGO-magnetite NCs Synthesize:

The composite was synthesized using via chemical co-precipitation approach. Primarily, ferrous ammonium sulphate ((NH<sub>4</sub>)<sub>2</sub>Fe(SO<sub>4</sub>)<sub>2</sub>·6H<sub>2</sub>O) is mixed with ferric chloride in a 1-2 molar ratio. The mixture is agitated mechanically for 30 minutes in 100ml of distilled water. After 30 minutes of ultrasonic treatment, various concentrations of RGO relative to magnetite (5, 10, and 30% wt. %) had been dissolved in 100 mL of distilled water. To prepare (MRG 5, 10, and 30%), each ratio of GO solution was separately poured to the iron solution, and the entire mixture was then agitated for a further 24 hours. In a separate 5L beaker, a sodium hydroxide solution (4L-15%) was prepared and heated to 90°C. After that, the ferrous, ferric, and RGO mixture was added to the hot NaOH solution [38].

### 2.4. Characterization:

UV-visible absorption spectrum was acquired by spectrophotometer (Agilent Cary UV-VIS) in the 200–800 nm range. (Bruker, Germany Alpha-p) FTIR with a diamond crystal sample cell and a maximum scanning depth of 2 μm was used to record an FT-IR spectrum in the range 4000–400 cm<sup>-1</sup>. The Raman spectrum was acquired at 2 cm<sup>-1</sup> resolution using Raman spectroscopy (model Sentera, Bruker, Germany with source (6.25 mW, 532nm neodymium-doped yttrium aluminum garnet (Nd:YAG) laser). On RGO/Fe<sub>3</sub>O<sub>4</sub> NCs, a 16+ mW laser power was irradiated to capture Raman spectra across a wide range of 4000–50 cm<sup>-1</sup>. (Bruker D8 ADVANCE X-ray diffractometer (Germany) with CuKα radiation, 40 KV, & 25 mA) was used to record XRD patterns. At an accelerating voltage of 200 kV, TEM pictures were taken using ((HRTEM) - model JEM-2100, JEOL, Japan). The sample's morphology was studied using a SEM (FEI Inspect S) equipped with EDX. Magnetism of RGO/Fe<sub>3</sub>O<sub>4</sub> Nano composites was investigated using a VSM (735VSM, Model7410; Lake Shore, Westerville, Ohio, USA).

### 2.5. Adsorption Studies:

Batch equilibrium approach was used to investigate the elimination of Cr (VI), Cu (II), and Mn (VII) using the 3 fabricated samples [46]. At room temperature of 24°C, 0.01 g of each sample was placed in 50 ml of appropriate concentration of metal ion solution in a separate 125 ml flask. At constant time intervals (15 mins) of adsorption, the effluent (3 ml) was separated from the synthesized sample by magnet, thereafter, centrifuged at 5000 rpm for 10 minutes to recover the adsorbent. The change in metal ion concentration against adsorption time was used to compute the adsorption rate of each metal ion, utilizing UV-Vis spectrum. As a reference, de-ionized water was employed [40].

The following equation was used to evaluate heavy metal removal:

$$\% \text{ Removal} = \frac{(C_i - C_e)}{C_i} \times 100 \quad (1)$$

Where:  $C_i$  is the heavy metals' initial concentration,  $C_e$  is the heavy metals' final concentration.

### 2.6. Adsorption Isotherms:

Langmuir & Freundlich isotherm was used to investigate the adsorption isotherm of RGO/Fe<sub>3</sub>O<sub>4</sub> NCs [39] [40] to compute optimum adsorption ability. As seen in (eq.2), Langmuir adsorption isotherm leads to constant adsorbent surface activation and mono-layer adsorption with selective adsorbent active sites.

$$q_e = \frac{q_m K_L C_e}{1 + K_L C_e} \quad (2)$$

Where:  $q_e$  Adsorbate amount adsorbed / adsorbent (gm) at equilibrium (mg/g),  $q_m$  Highest adsorption capacity (mg/g),  $K_L$  Isotherm constant of Langmuir (L/mg) &  $C_e$  Concentration of adsorbate at equilibrium (mg/L)

Freundlich isotherm denotes adsorbent surface heterogeneity along with surface multilayered coverage. The linear Freundlich isotherm equation is as follows as (eq.3).

$$\log q_e = \log K_F + \frac{1}{n} \log C_e \quad (3)$$

Where:  $K_F$  Freundlich coefficient indicates the relative adsorption capability of an adsorbent &  $n$  Freundlich coefficient indicating adsorption strength.

### 2.7. Adsorption Kinetics:

When defining the adsorption mechanism, the physical and chemical properties of the adsorbent, as well as diffusion mechanisms, are two of the most significant parameters to examine. The mechanism of the adsorption sequence was investigated by applying pseudo-first-order and pseudo-second-order kinetics on the experimental results in order to evaluate the impact of adsorption time on removal of heavy metals with RGO/Fe<sub>3</sub>O<sub>4</sub> NCs. Heavy metal The RGO/ Fe<sub>3</sub>O<sub>4</sub> NCs adsorption equilibrium timeframe was 200 minutes. In (eq.4), The pseudo first order kinetic model of Langergren is denoted by [41].

$$\ln(q_e - q_t) = \ln q_e - k_1 t \quad (4)$$

Where:  $q_e$  &  $q_t$  Adsorbate quantities adsorbed / gm of adsorbent at equilibrium and over time (t) (mg/g) &  $k_1$  First order adsorption Langergren rate constant ( $\text{min}^{-1}$ ), calculated by graphing  $\ln(q_e - q_t)$  against (t).

As formulated (eq.5), the pseudo-second-order kinetics is [42]

$$\frac{t}{q_t} = \frac{1}{k_2 q_e^2} + \frac{t}{q_e} \quad (5)$$

Where:  $k_2$  Adsorption rate constant of second order (g/mg.min), derived from the plotted graph of  $\frac{t}{q_t}$  Vs t intercept.

## 3. RESULTS & DISCUSSION

### 3.1. Synthesized nano-composites Characterization:

#### 3.1.1. Results of Scanning Electron Microscope (SEM analysis & Energy Dispersive Analysis X-ray (EDXA analysis):

The SEM images with EDXA characterization of the 30% composite are shown in Figure 1.

The SEM revealed crystalline aggregation of relatively typical globular shape particles of varied crystal size. EDXA mapping of composite, on the other hand, revealed the existence of  $K_\alpha$  radiation of C, O, Fe Na and Si. Presence of (C & O) validates existence of RGO, while the presence of (Fe) element proves the presence of magnetite.

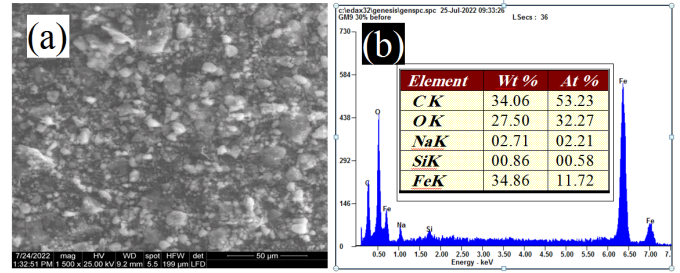


Figure 1: SEM micrograph and EDAX analysis of MRG30

#### 3.1.2. Results of High-Resolution Transmission electron microscope (HRTEM)

Magnetite morphologies with various percentages of reduced graphene oxide (5%, 10%, and 30%) were shown in Figure.2. As depicted, the grey region displays RGO nanoparticles, whereas the black portion depicts Fe<sub>3</sub>O<sub>4</sub> nanoparticle aggregates. Magnetite is vividly visible in MRG (5 percent & 10 percent respectively). Graphene, on the other hand, has a tendency to cover the entire nanoparticle at MRGO 30%, reducing their activity.

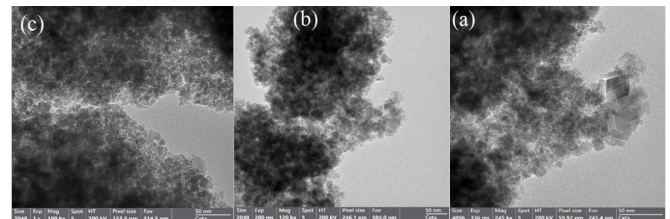


Figure 2: TEM of (a) RGO5%, (b) RGO10% & (c) RGO30%.

#### 3.1.3. Results of X-Ray diffraction (XRD analysis):

Magnetite was mounted on reduced graphene oxide in varied ratios. X-ray diffraction (XRD) was primarily used to investigate the magnetic reduced graphene nanocomposite crystalline phase. Diffraction peaks at  $2\theta$  of (30.27, 35.75, 43.6, 53.73, 57.5, and 63.1), respectively, are associated with the cubic Fe<sub>3</sub>O<sub>4</sub> crystal plane [(220), (311), (400), (422), (440), (511), and (511), respectively] as represented in fig. 3. There were no peaks of reduced graphene oxide detected for two reasons: (a) we think that the presence of magnetite limits graphene sheet aggregation. (b) The strong signal of iron oxides likely overwhelms the graphene's weak peak.

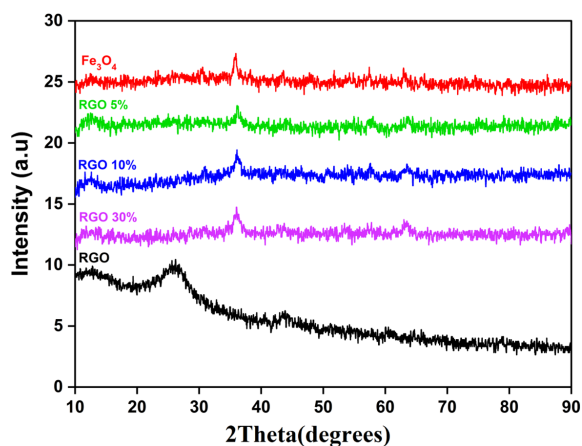


Figure 3: Difference in XRD results of:  $\text{Fe}_3\text{O}_4$ , RGO 5% , RGO 10%, RGO 30% and RGO.

### 3.1.4. Dispersive Raman spectroscopy analysis:

As shown in fig. 4, G & D peaks are considered as fundamental precepts of graphitic carbon-based materials' Raman spectra. Raman spectra frequently contained D band at  $1337\text{cm}^{-1}$  and a G band at  $1570\text{cm}^{-1}$ . The intensity of D peak is used commonly to assess the magnitude of disorder. The change and shape of D peak's overtone, referred to by the 2D peak about  $2660\text{cm}^{-1}$  [43], possibly be correlated with the number of layers of graphene (N).

As seen in Fig. (4), there are three peaks in the Raman spectra of MRGx (where x is 5, 10&30) that associated with  $\text{Fe}_3\text{O}_4$  nanoparticles. The big peaks detected at  $1357$  &  $1592\text{cm}^{-1}$  attributable to D and G of RGO, respectively [44].  $I_D/I_G$  ratio in RGO is 0.97. MRG5, MRG10, & MRG30 still have 2 distinct G & D band peaks, but the  $I_D/I_G$  ratios found to be 1.52, 1.23, and 1.375. The significantly greater intensity of the D band in composites than the G band is evidence of presence of  $\text{sp}^3$  defects in  $\text{sp}^2$  throughout graphene decoration by magnetite and vigorous exfoliation of RGO sheets. This demonstrates successful graphene exfoliation along with the replacement of oxygen in the GO by  $\text{Fe}_3\text{O}_4$  during reduction., resulting in a chemical bond between  $\text{Fe}_3\text{O}_4$  and RGO [45].

### 3.1.5. Results of Fourier transform infrared spectroscopy (FTIR analysis)

FTIR spectrum, showing in Fig.5, demonstrated an effective inclusion of RG sheets in the  $\text{Fe}_3\text{O}_4$

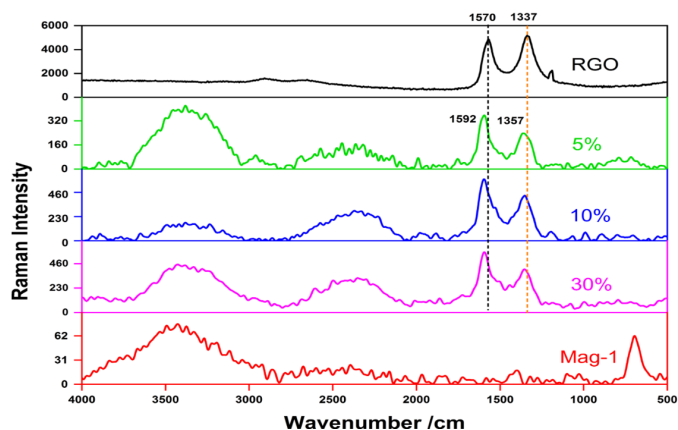


Figure 4: Raman Spectra (RGO, RGO 5%, RGO 10%, RGO 30% and  $\text{Fe}_3\text{O}_4$ )

nanoparticles. The wide peak at approximately ( $3400\text{cm}^{-1}$ ) was attributed to the O-H bond stretching vibration. absorption peak around ( $600\text{cm}^{-1}$ ) is related to the combination of Fe-O vibrations, illustrating a successful mixing of RG sheets and  $\text{Fe}_3\text{O}_4$  nanoparticles [46]. The appearance of an absorption band around ( $1552\text{cm}^{-1}$ ) serves as proof that RGO was created, which is related to the RGO sheets' skeletal vibration [47].

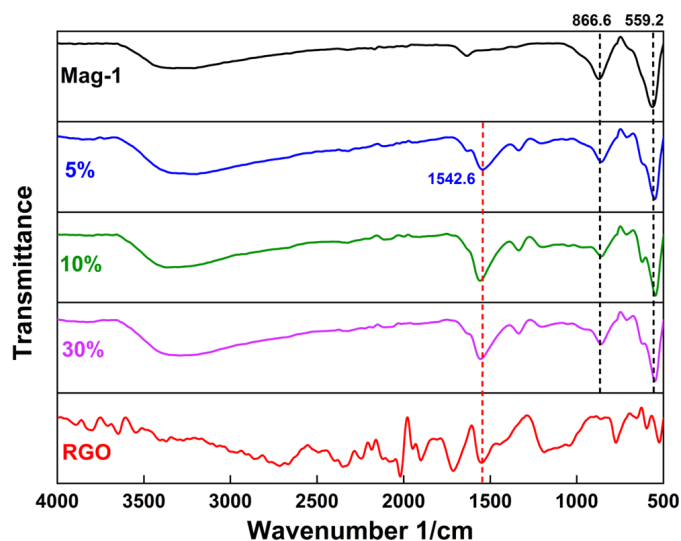


Figure 5: FTIR Spectra (RGO, RGO 5%, RGO 10%, RGO 30% and  $\text{Fe}_3\text{O}_4$ )

### 3.1.6. Vibrating Sample Magnetometer (VSM analysis):

VSM was performed at room temp., and the magnetic properties of MRG 10, 20 & 30samples is

depicted as shown in Fig (6). Magnetization hysteresis loops with S-like curves are seen in  $\text{Fe}_3\text{O}_4$  nanoparticles and MRG nanocomposites. MRG 5, 10, and 30 samples all showed superparamagnetic properties and values of saturation magnetizations (50, 47.3 & 40.6) emu/g. The findings demonstrate appropriate magnetism for the simple use of a magnet to separate the Nano composites from the solution and reusing them in other operations.

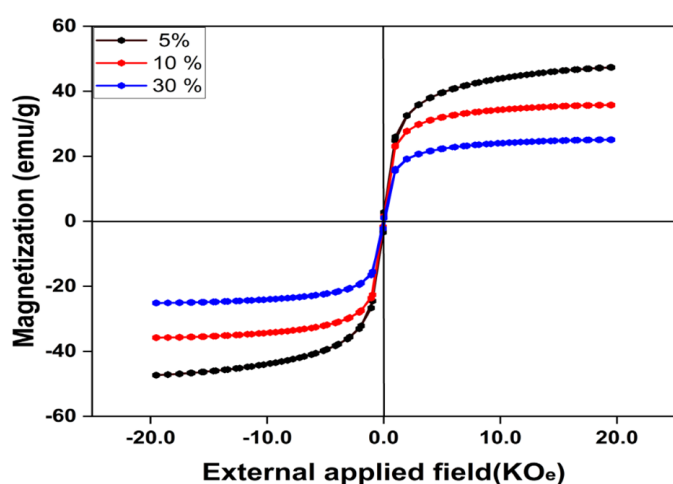


Figure 6: VSM measurements for magnetic nanoparticles, of MRG5, MRG 10 and MRG30.

### 3.2. Removal performance of RGO and magnetite nanocomposites toward Cr (VI), Cu (II) and Mn (VII) heavy metals:

The adsorption has been evaluated spectrophotometrically at the highest absorption (viz.  $\lambda_{max}$  = 372, 523 and 800 nm) relating to Cr (VI), Mn (VII) & Cu(II) matching well with early-declared findings (Fig. 7) [48]. To evaluate the adsorption influence of the designed adsorbents, Cr (VI), Cu (II) & Mn (VII) was used as a model heavy metals contaminants in this study. Figure 8 shows different adsorption efficiency toward heavy metals by using virgin RGO,  $\text{Fe}_3\text{O}_4$ , MRG5, MRG10 and MRG30 nanocomposite. The RGO shows only 23.5, 33 and 27.5 % after 120 min adsorption for Cr (VI), Cu (II) & Mn (VII), meanwhile the highest adsorption activity achieved by  $\text{Fe}_3\text{O}_4$  was 29.5, 40 and 36.5 % after 120 min adsorption for Cr (VI), Cu (II) & Mn (VII) respectively, on contrary highest adsorption activ-

ity can be achieved by MRG30 of Cr (VI), Cu (II) & Mn (VII) was 50.5, 77, 63 % after the same time.

#### 3.2.1. Dosage of adsorbent effect:

Dose of the adsorbents is one of the factors that significantly influences the adsorption capability. To study the impact of amount of adsorbent on the adsorption of Cr (VI), Cu (II) & Mn (VII) on MRG30, the experiments were performed with various amounts of MRG30: 5.0, 10.0 & 20.0 mg  $\text{L}^{-1}$ . Fig. 9 displays the findings that were achieved. These findings demonstrate that as the quantity of adsorbent is increased, heavy metal adsorption onto MRG30 rises. The possibility that the adsorption sites progress and continue to stay unsaturated throughout the adsorption process, increasing the probability of adsorption, is one of the possible explanations for this hypothesis [49, 50]. Active centers are the name given to such sites. Surface area & average pores available after adsorption are related to the intensity of these sites on adsorbent's surface. This clarifies how adsorption increased when the amount of adsorbent was increased.

#### 3.2.2. Metal Ion's Initial Concentration Effect:

Because the initial concentration of Cr (VI), Cu (II) & Mn (VII) metal ions is crucial to the removal process, the impact of metal ion ionic strength was investigated by varying the initial concentration while maintaining the other reaction conditions. Fig. 10 shows how removal percentage varies with contact time at various initial concentrations (5, 10 and 20 mg/l). At higher concentration of Cr (VI), Cu (II) & Mn (VII) metal ions, it was noted that the removal percentage was lower than that of the lower initial concentration. This is due to the heavy metal ions' obstruction of approaching the adsorbent's surface area. Surface area and abundance of adsorption sites were comparatively high at low starting solution concentration, making it simple to adsorb and increase the heavy metal removal %. The total number of adsorption sites that are reachable is constrained at higher starting solution concentrations, which causes a reduction in the percentage of heavy metal ion removal [51, 52].

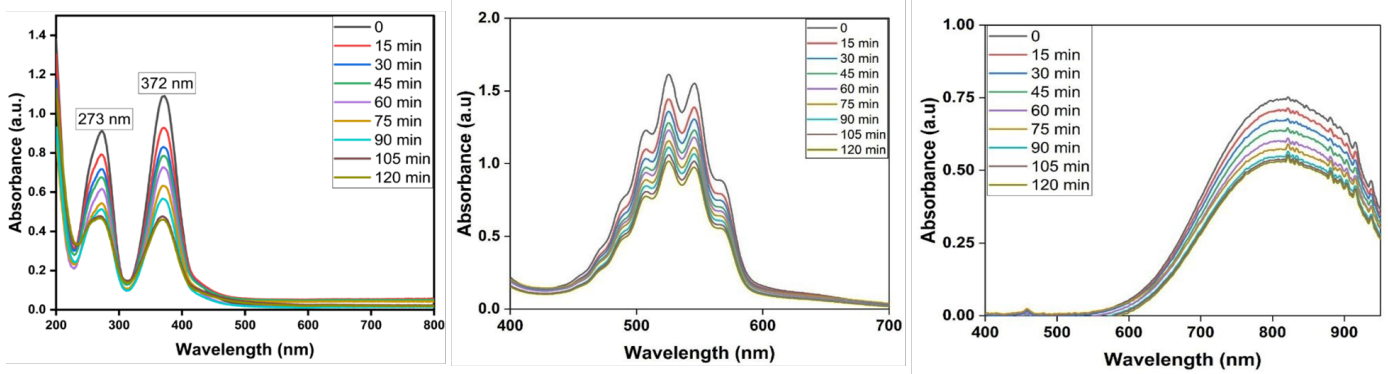


Figure 7: UV-Visible spectra for (a) Cr (VI), (b) Mn (VII) & (c) Cu (II) at different concentrations with time intervals.

### 3.2.3. pH Effect:

PH of the solution is a critical factor for removal studies. The impact of the metal ions solution's initial pH values was studied for 120 minutes under specified experimental circumstances (MRG30 nanocomposite 10 mg, 50 ml of a  $20 \text{ mgL}^{-1}$  of Cr (VI) and Mn(VII) &  $100 \text{ mg/L}$  of Cu(II)solution, at

$T = 25^\circ \text{C}$ ). Fig. 11 is a graph illustrating the variation in metal removal percentage over time at different pH values for the solution (3.0 – 9.0). The highest removal activity for all studied metals was recorded at pH 9.0. Adsorbent's point of zero charge determination may explain why the adsorption activity have maximum at higher pH values. To confirm

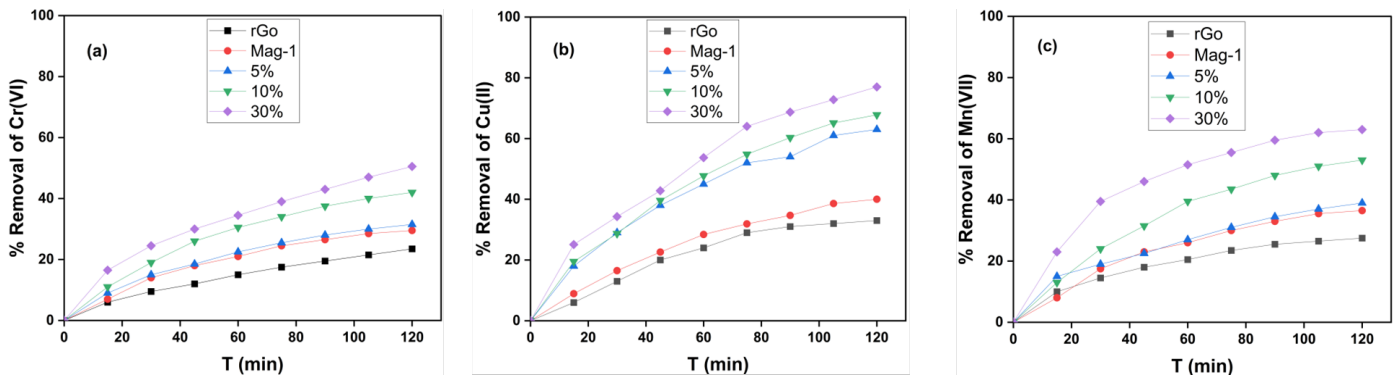


Figure 8: Screening the adsorption behavior of RGO,  $\text{Fe}_3\text{O}_4$ , MRG5, MRG10 and MRG30 respectively against 50 ml metal ions solution of (a) Cr (VI)  $20 \text{ mgL}^{-1}$ , (b) Cu(II)  $100 \text{ mgL}^{-1}$  & (c) Mn(VII)  $20 \text{ mgL}^{-1}$  at  $T = 25^\circ \text{C}$  and pH 7.

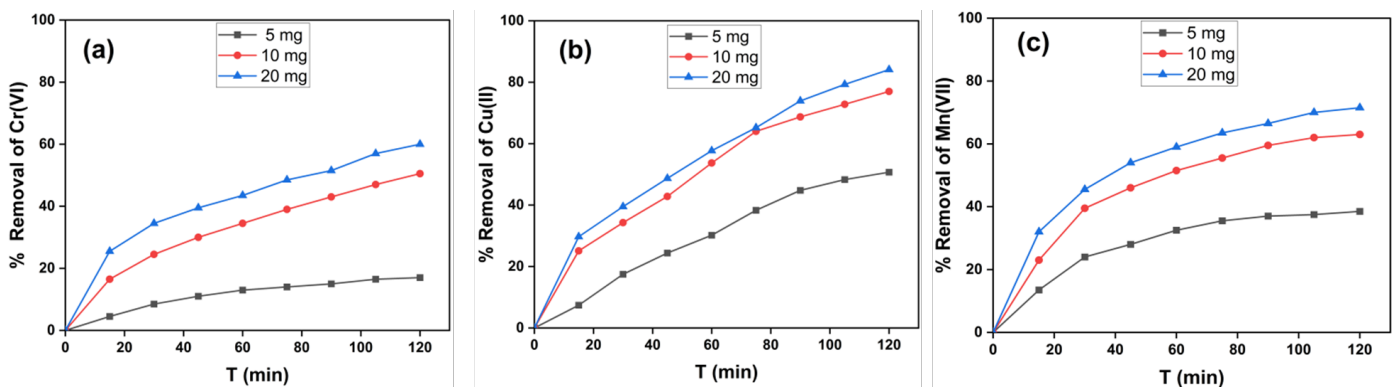


Figure 9: Effect of the dosage of adsorbent on the efficiency of removal of metal ions of (a) Cr (VI), (b) Cu(II) & (c) Mn(VII) with at  $T = 25^\circ \text{C}$  and pH 7)

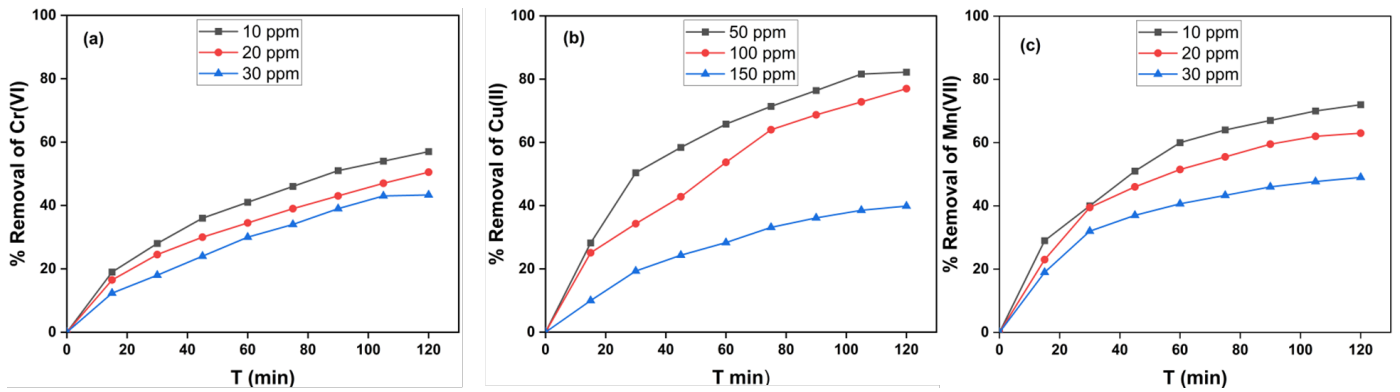


Figure 10: Differences of removal percentage with contact time as a function at various initial concentrations of metal ions (a) Cr (VI), (b) Cu (II) & (c) Mn (VII) at pH 7 and 10.0 mg MRG30 nanocomposite

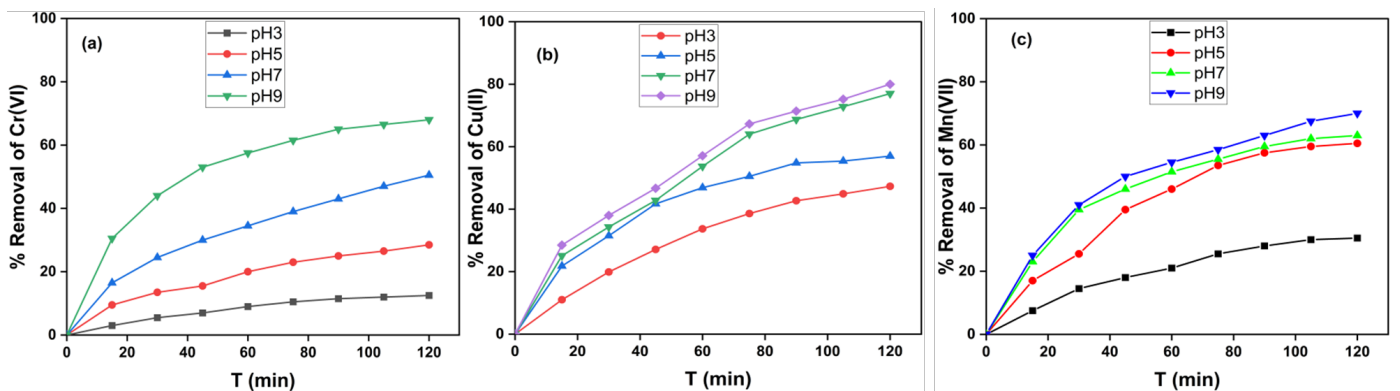


Figure 11: Removal percent with time at different solution pH values (3.0 – 9.0) for (a) Cr (VI), (b) Cu(II) & (c) Mn(VII)

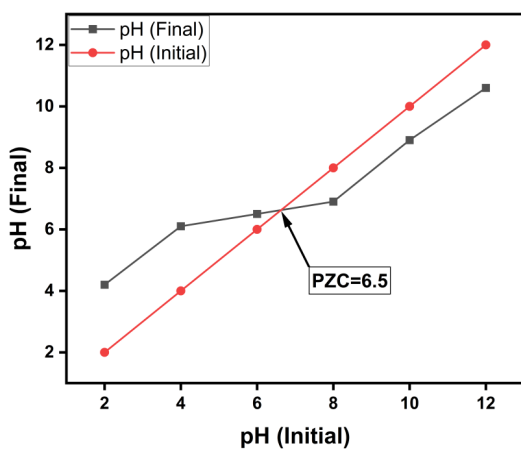


Figure 12: (PZC) Point of zero charge of MRG30 nano-composite

the MRG30 nano-composite’s point of zero charges (PZC), 0.01 g was added to a 50 mL solution 0.01 M NaCl. HCl or NaOH were used to adjust the pH lev-

els of the solutions at values (2, 4, 6, ... 12). The samples have been stirred at 200 rpm for 48 hours. After separating MRG30 nano-composite, the solutions’ pH values were recorded. Using a graph that compares the end pH to the beginning pH, the PZC value was calculated. The PZC was found to be 6.5 (when there is no discernible difference between the final and initial pH readings) as depicted in Fig. 12. When pH is lower than pH of PZC, it means that the MRG30 surface is positively charged and when pH is greater than pH of PZC, it means that the MRG30 surface is negatively charged. In addition, when pH (solution) = the pH of PZC, The MRG30 has a neutral surface charge, and the metals ions’ electrostatic attraction to the surface of the adsorbent is very weak. [53]. PH value of PZC with respect to MRG30 was found to be 6.5, and this discovery clarified why, as shown in Fig. 11, the removal of metals was greatest at pH 9.0. Consequently, at this point, the MRG30 nano-composite’s

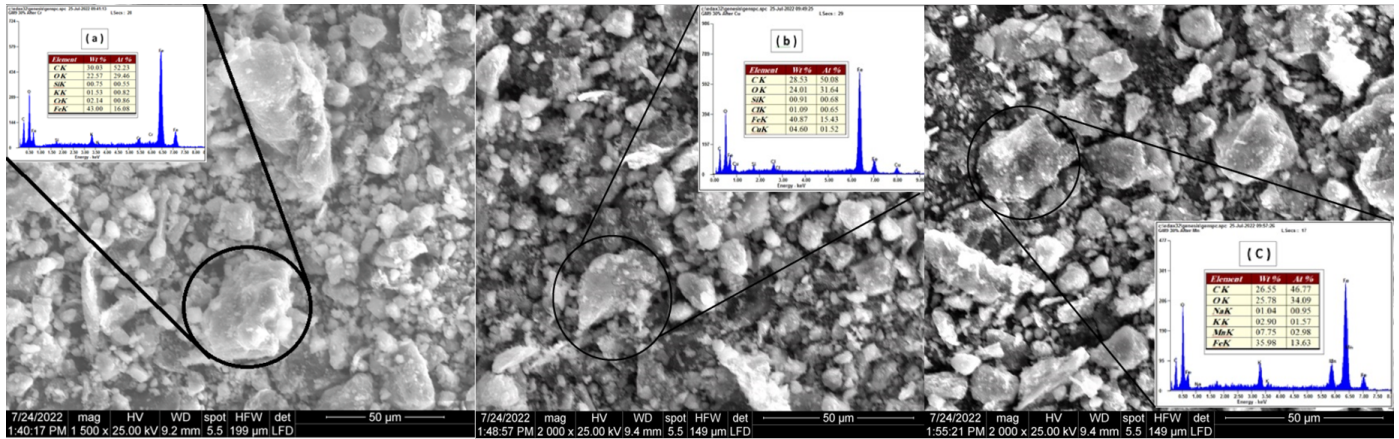


Figure 13: SEM and EDAX analysis of MRG30 after adsorption process.

net surface charge is negative, attracting the positively charged Cr (VI), Cu (II) & Mn (VII) and enhancing the adsorption activity. At pH lower than 6.5, the % removal started to decrease due to the repulsion between the positive surface charges of metals and the MRG30 nano-composite's positive net surface charges.

### 3.2.4. Kinetic studies:

The linear form of the pseudo-first order equation

$$\log(q_e - q_t) = \log q_e - k_1 t \quad (6)$$

Where:  $q_e$  &  $q_t$ ; Quantities of adsorbate adsorbed per gram of adsorbent at equilibrium and throughout time (t) (mg/g),  $k_1$ ; removal rate constant, and t; time of removal.

Fig. 1S depicts a graphing  $\ln(q_e - q_t)$  against t. The results showed the metal ions under investigation don't give straight lines and consequently don't comply the pseudo-first order Langergren equation which make it not suitable to describe the adsorption process of the studied metal ions on the synthesized nano-composite.

The linear form of the pseudo-second order equation:

$$\frac{t}{q_t} = \frac{1}{k_2 q_e^2} + \frac{t}{q_e} \quad (7)$$

Where:  $k_2$ : The second-order adsorption rate constant (g/mg.min), which can be calculated from the intercept of the  $\frac{t}{q_t}$  vs t linear plot

As revealed in Fig. 2S, the finding showed straight line relation with good  $R^2$  correlation coefficient values indicating that the removal process' kinetics adhered to the laws for pseudo-second-order. Moreover the apparent pseudo-second-order rate constants are reduced as the concentration of heavy metal ions rises. This dependence on Cr (VI), Cu(II) and Mn (VII) ions concentration as a function of reaction rate constants is consistent with the literature [53, 54].

### 3.2.5. SEM and EDAX after adsorption:

Following the metal ion uptake, the composite conducted SEM and EDXA studies, which showed considerable morphological and microstructural variations. Additionally, EDXA data showed that the composite included Cr (VI), Cu (II) and Mn (VII) ions, demonstrating that the heavy metal ions had made contact with the nano-composite's surface as shown in **Figure 13**.

## 4. Conclusion:

This study investigated the outstanding heavy metal removal activity of reduced graphene oxide/magnetite nano-composite. XRD, HRTEM, SEM, EDXA, Raman, FTIR, and VSM analysis techniques are used to characterize RGO, and RGO/ magnetite nanocomposite MRG revealing the chemical composition and the morphological properties of the composite with finding the superparamagnetic properties and values of saturation magnetizations. From the results of uptaking the

heavy metal ions by adsorption on the synthesized nano-composite, we suggested that there is a synergistic effect takes place between both of RGO and magnetite resulting that the RGO/magnetite nano-composite have higher adsorption efficiency than both RGO and magnetite itself and the highest removal percent (80, 70 and 68 %) for Cu (II), Mn (VII) & Cr (VI) respectively was achieved with pH 9.0 because at this pH value the surface net charge of the nano-composite is -ve since the PZC of the composite was measured and found to be 6.5, so there is electrostatic attraction between the negatively charged adsorbent and the positively charged metal ions. In addition, the study showed that the adsorption efficiency of MRG 30 found to be highest among other MRG composites. Due to its highly efficient adsorption activity, MRG30 nanocomposite has the potential to serve as a useful adsorbent in water treatment to preserve our environment from hazardous contaminants.

#### Acknowledgments:

The authors deeply thanks **Dr. Ahmed M. El-khawaga**, faculty of medicine, Galala University for his help and assistance throughout the study.

#### References

- [1] J. Y. Lim, Recent trends in the synthesis of graphene and graphene oxide based nanomaterials for removal of heavy metals-A review, *Journal of Industrial and Engineering Chemistry* 66 (2018) 29–44.
- [2] M. U. Tahir, et al., Preparation of hydroxypropyl-cyclodextrin-graphene/Fe<sub>3</sub>O<sub>4</sub> and its adsorption properties for heavy metals (2019).
- [3] H. Zeng, et al., Efficient adsorption of Cr (VI) from aqueous environments by phosphoric acid activated eucalyptus biochar, *Journal of Cleaner Production* 286 (2021) 124964–124964.
- [4] S. Begum, Review of chitosan composite as a heavy metal adsorbent: Material preparation and properties. *Carbohydrate polymers* (2021).
- [5] I. Medha, et al., -Aminopropyl) triethoxysilane and iron rice straw biochar composites for the sorption of Cr (VI) and Zn (II) using the extract of heavy metals contaminated soil. *Science of The Total Environment* (2021).
- [6] G. K. R. Angaru, Facile synthesis of economical feasible fly ash-based zeolite-supported nano zerovalent iron and nickel bimetallic composite for the potential removal of heavy metals from industrial effluents, *Chemosphere* 267 (2021) 128889–128889.
- [7] H. Masoumi, A. Ghaemi, H. G. Gilani, Evaluation of hyper-cross-linked polymers performances in the removal of hazardous heavy metal ions: A review. *Separation and Purification Technology* (2021).
- [8] J. Zhang, A key role of inner-cation- $\pi$  interaction in adsorption of Pb (II) on carbon nanotubes: Experimental and DFT studies, *Journal of Hazardous Materials* 412 (2021) 125187–125187.
- [9] Y. Pan, Stable self-assembly AgI/UiO-66 (NH<sub>2</sub>) heterojunction as efficient visible-light responsive photocatalyst for tetracycline degradation and mechanism insight, *Chemical Engineering Journal* 384 (2020) 123310–123310.
- [10] J. Zhang, Core-shell Ag@ nitrogen-doped carbon quantum dots modified BiVO<sub>4</sub> nanosheets with enhanced photocatalytic performance under Vis-NIR light: Synergism of molecular oxygen activation and surface plasmon resonance, *Chemical Engineering Journal* 410 (2021) 128336–128336.
- [11] X. Weng, Impact of synthesis conditions on Pb (II) removal efficiency from aqueous solution by green tea extract reduced graphene oxide, *Chemical Engineering Journal* 359 (2019) 976–981.
- [12] L. Jin, Preparation of stable and high-efficient poly (m-phenylenediamine)/reduced graphene oxide composites for hexavalent chromium removal, *Journal of Materials Science* 54 (1) (2019) 383–395.
- [13] M. Gao, Novel magnetic graphene oxide decorated with persimmon tannins for efficient adsorption of malachite green from aqueous solutions, *Colloids and Surfaces A: Physicochemical and Engineering Aspects* 566 (2019) 48–57.
- [14] M. U. Farooq, M. I. Jalees, Application of magnetic graphene oxide for water purification: heavy metals removal and disinfection, *Journal of Water Process Engineering* 33 (2020) 101044–101044.
- [15] D. Huang, Novel insight into adsorption and co-adsorption of heavy metal ions and an organic pollutant by magnetic graphene nanomaterials in water, *Chemical Engineering Journal* 358 (2019) 1399–1409.
- [16] Q. Kong, Fabrication of terminal amino hyperbranched polymer modified graphene oxide and its prominent adsorption performance towards Cr (VI), *Journal of hazardous materials* 363 (2019) 161–169.
- [17] M. Ghobadi, MnFe<sub>2</sub>O<sub>4</sub>-graphene oxide magnetic nanoparticles as a high-performance adsorbent for rare earth elements: synthesis, isotherms, kinetics, thermodynamics and desorption, *Journal of hazardous materials* 351 (2018) 308–316.
- [18] C. R. Minitha, et al., Magnetite nanoparticle decorated reduced graphene oxide composite as an efficient and recoverable adsorbent for the removal of cesium and strontium ions. *Industrial & Engineering Chemistry Research* (2018).
- [19] H. Hosseinzadeh, S. Ramin, Effective removal of copper from aqueous solutions by modified magnetic chi-

- tosan/graphene oxide nanocomposites, *International journal of biological macromolecules* 113 (2018) 859–868.
- [20] Y. Liu, Synthesis of magnetic polyaniline/graphene oxide composites and their application in the efficient removal of Cu (II) from aqueous solutions, *Journal of environmental chemical engineering* 4 (1) (2016) 825–834.
- [21] F. E. Peer, N. Bahramifar, H. Younesi, Pb (II) and Cu (II) ions from aqueous solution by polyamidoamine dendrimer grafted magnetic graphene oxide nanosheets, *Removal of Cd (II)* 87 (2018) 225–240.
- [22] Z. F. Yang, Fabrication of magnetic iron oxide@graphene composites for adsorption of copper ions from aqueous solutions, *Materials Chemistry and Physics* 219 (2018) 30–39.
- [23] W. S. Hummers, R. E. Offeman, Preparation of graphitic oxide, *Journal of the american chemical society* 80 (6) (1958) 1339–1339.
- [24] H. Zhang, Fabrication of methyl acrylate and tetraethylenepentamine grafted magnetic chitosan microparticles for capture of Cd (II) from aqueous solutions, *Journal of hazardous materials* 366 (2019) 346–357.
- [25] A. Sherlala, Adsorption of arsenic using chitosan magnetic graphene oxide nanocomposite, *Journal of environmental management* 246 (2019) 547–556.
- [26] S. Banerjee, et al., Graphene oxide (rGO)-metal oxide (TiO<sub>2</sub>/Fe<sub>3</sub>O<sub>4</sub>) based nanocomposites for the removal of methylene blue. *Applied surface science* (2018).
- [27] P. Benjwal, et al., Enhanced photocatalytic degradation of methylene blue and adsorption of arsenic (iii) by reduced graphene oxide (rGO)-metal oxide (TiO<sub>2</sub>/Fe<sub>3</sub>O<sub>4</sub>) based nanocomposites (2015).
- [28] Z. Geng, Highly efficient dye adsorption and removal: a functional hybrid of reduced graphene oxide-Fe<sub>3</sub>O<sub>4</sub> nanoparticles as an easily regenerative adsorbent, *Journal of Materials Chemistry* 22 (8) (2012) 3527–3535.
- [29] A. Meidanchi, O. Akhavan, Superparamagnetic zinc ferrite spinel-graphene nanostructures for fast wastewater purification. *Carbon* (2014).
- [30] V. Chandra, Water-dispersible magnetite-reduced graphene oxide composites for arsenic removal, *ACS nano* 4 (7) (2010) 3979–3986.
- [31] Z. Niu, Spin transport in magnetic graphene superlattices, *The European Physical Journal B* 66 (2) (2008) 245–250.
- [32] T. Qi, Synthesis, characterization and adsorption properties of magnetite/reduced graphene oxide nanocomposites, *Talanta* 144 (2015) 1116–1124.
- [33] N. T. V. Hoan, Fe<sub>3</sub>O<sub>4</sub>/reduced graphene oxide nanocomposite: synthesis and its application for toxic metal ion removal, *Journal of Chemistry* (2016).
- [34] O. Duman, Removal of triphenylmethane and reactive azo dyes from aqueous solution by magnetic carbon nanotube- $\kappa$ -carrageenan-Fe<sub>3</sub>O<sub>4</sub> nanocomposite, *Journal of Alloys and Compounds* 687 (2016) 370–383.
- [35] O. Duman, et al., Synthesis of magnetic oxidized multiwalled carbon nanotube- $\kappa$ -carrageenan-Fe<sub>3</sub>O<sub>4</sub> nanocomposite adsorbent and its application in cationic Methylene Blue dye adsorption. *Carbohydrate polymers* (2016).
- [36] D. C. Marcano, Improved synthesis of graphene oxide, *ACS nano* 4 (8) (2010) 4806–4814.
- [37] S. Abdolhosseinzadeh, H. Asgharzadeh, H. S. Kim, Fast and fully-scalable synthesis of reduced graphene oxide. *Scientific reports* (2015).
- [38] D. Li, et al., Determination of trace bisphenol A in environmental water by high-performance liquid chromatography using magnetic reduced graphene oxide based solid-phase extraction coupled with dispersive liquid-liquid microextraction. *Analytical and bioanalytical chemistry* (2017).
- [39] X. Chen, Modeling of experimental adsorption isotherm data. *information* (2015).
- [40] N. Ghasemi, Adsorption isotherms and kinetics studies for the removal of Pb (II) from aqueous solutions using low-cost adsorbent, *Proceedings of the International Conference on Environment Science and Engineering* (2012).
- [41] S. Lagergren, Zur theorie der sogenannten adsorption gelöster stoffe. *Kungliga svenska vetenskapsakademiens. Handlingar*, 1898.
- [42] D. Robati, Pseudo-second-order kinetic equations for modeling adsorption systems for removal of lead ions using multi-walled carbon nanotube, *Journal of nanostructure in Chemistry* (3) (2013) 1–6.
- [43] L. Shahriary, A. A. Athawale, Graphene oxide synthesized by using modified hummers approach, *Int. J. Renew. Energy Environ. Eng* 2 (01) (2014) 58–63.
- [44] J. Cheng, Influence of component content on the capacitance of magnetite/reduced graphene oxide composite, *Journal of Electroanalytical Chemistry* 698 (2013) 1–8.
- [45] H. H. El-Maghrabi, Magnetic graphene based nanocomposite for uranium scavenging, *Journal of hazardous materials* 322 (2017) 370–379.
- [46] Y. Gao, Thermal regeneration of recyclable reduced graphene oxide/Fe<sub>3</sub>O<sub>4</sub> composites with improved adsorption properties, *Journal of Chemical Technology & Biotechnology* 89 (12) (2014) 1859–1865.
- [47] S. Shah, M. S. A, Green synthesis of biphasic TiO<sub>2</sub>-reduced graphene oxide nanocomposites with highly enhanced photocatalytic activity, *ACS applied materials & interfaces* 4 (8) (2012) 3893–3901.
- [48] S. Laouini, A. Bouafia, M. Tedjani, Catalytic activity for dye degradation and characterization of silver/silver oxide nanoparticles green synthesized by aqueous leaves extract of *Phoenix dactylifera* L (2021).
- [49] B. Abbar, et al., Experimental investigation on removal of heavy metals (Cu<sup>2+</sup>, Pb<sup>2+</sup>, and Zn<sup>2+</sup>) from aqueous solution by flax fibres, *Process Safety and Environmental Protection* 109 (2017) 639–647.
- [50] B. Yu, et al., The removal of heavy metal from aqueous

ous solutions by sawdust adsorption-removal of copper, *Journal of hazardous materials* 80 (1-3) (2000) 33–42.

- [51] A. H. A. Saad, et al., Removal of toxic metal ions from wastewater using ZnO@ Chitosan core-shell nanocomposite. *Environmental Nanotechnology, Monitoring & Management* (2018).
- [52] M. A. Elkodous, et al., Enhanced photocatalytic and antimicrobial performance of a multifunctional Cu-loaded nanocomposite under UV light: theoretical and experimental study, *Nanoscale* 10 (4) (2018) 1549–2172.
- [53] R. Gusain, et al., Adsorptive removal and photocatalytic degradation of organic pollutants using metal oxides and their composites: A comprehensive review (2019).
- [54] R. E. Adam, et al., Synthesis of ZnO nanoparticles by coprecipitation method for solar driven photodegradation of Congo red dye at different pH (2018).